Heliyon 10 (2024) e32863

Contents lists available at ScienceDirect

Heliyon

journal homepage: www.cell.com/heliyon

Research article

Impacts of designed vanillic acid-polymer-magnetic iron oxide nanocomposite on breast cancer cells

Farahnaz Barahuie [a], Dena Dorniani [b], Bullo Saifullah [c], Palanisamy Arulselvan [d], Mohd Zobir Hussein [e,*], Ravindran Jaganathan [f], Fawzi Mohamed Amin El-Fagaih [g], Ariyati Retno Pratiwi [e]

[a] Faculty of Industry & Mining (Khash), University of Sistan and Baluchestan, Zahedan, Iran
[b] Chemistry Department, University of Sheffield, Dainton Building, Brook Hill, Sheffield, S3 7HF, UK
[c] Department of Human and Rehabilitation Sciences, The Begum Nusrat Bhutto Women University, Sukkur, Sindh, Pakistan
[d] Department of Chemistry, Saveetha School of Engineering, Saveetha Institute of Medical and Technical Sciences (SIMATS), Saveetha University, Chennai, Tamil Nadu, 602 105, India
[e] Faculty of Dentistry, Brawijaya University, Malang, Indonesia
[f] Microbiology Unit, Preclinical Department, Faculty of Medicine, University Kuala Lumpur, Royal College of Medicine Perak (UniKL-RCMP), Ipoh-30450, Perak, Malaysia
[g] Department of Chemical and Petrochemical Engineering, The College of Engineering & Architecture, Initial Campus, Birkat Al Mouz Nizwa, Oman

ARTICLE INFO

Keywords:
Nanocomposite
Vanillic acid
Chitosan
Anticancer nano-delivery
Breast cancer

ABSTRACT

The engineered nano-vehicle was constructed using magnetic iron oxide nanoparticles (MIONs) and chitosan (CTS) to stabilize anticancer agent vanillic acid (VNA) which was loaded on CTS-coated MIONs nanocarrier, and more importantly, to achieve sustained VNA release and subsequent proper anticancer activity. The new thermally stable VNA-CTS- MIONs nanocomposite was spherical with a middle diameter of 6 nm and had a high drug loading of about 11.8 %. The MIONs and resulting nanocomposite were composed of pure magnetite and therefore, were superparamagnetic with saturation magnetizations of 53.3 and 45.7 emu.g^{-1}, respectively. The release profiles of VNA from VNA-CTS-MIONs nanocomposite in different pH values were sustained and showed controlled pH-responsive delivery of the loaded VNA with 89 % and 74 % percentage release within 2354 and 4046 min at pH 5 and 7.4, respectively, as well as were in accordance with the pseudo-second-order model. The VNA-CTS-MIONs nanocomposite treatment at diverse concentrations remarkably decreased the viability and promoted ROS accumulation and apoptosis in the MDA-MB-231 breast cancer cells. Hence, it can be a propitious candidate for the management of breast cancer in the future.

1. Introduction

Breast cancer, the most common malignancy in women, had a major impact on the patient's physical and mental health. It was the prime reason for cancer death amid women around the globe [1]. Breast cancer treatment options included surgical removal of the tumor, chemotherapy, radiation, and hormone therapy. Despite the availability of many chemotherapeutic medications, the capability of cancerous cells to gain resistance toward these drugs posed a significant problem for cancer treatment [2]. Additionally, the tumor

* Corresponging author.
E-mail address: mzobir28@gmail.com (M.Z. Hussein).

https://doi.org/10.1016/j.heliyon.2024.e32863
Received 4 March 2024; Received in revised form 9 June 2024; Accepted 11 June 2024
Available online 12 June 2024

cells possessed relapse or distant metastasis because of the drug resistance and toxicity. About 30 % of patients treated in the early stages relapse, despite the availability of several therapeutic methods such as chemotherapy, hormone therapy, and radiotherapy [3]. Consequently, the new therapeutic approaches against breast cancer might benefit public health.

Developments in nanotechnology have endowed the design of nanodrugs and drug nano-vehicles that could increase drug half-life, traverse various biological barriers, and target specified diseased areas. Cancer was denoted a crucial performer when it reached the nanotechnology biomedical usages, particularly through nanoparticle drug delivery systems [4–7]. In contrast with large-scale drug delivery systems of restrained efficacy, nanoparticle drug delivery systems afforded myriad benefits like prolonged release of drugs, lowered toxicity, enhanced targeting ability, and improved cellular uptake, displaying abundant potential in cancer therapy [8–10]. Current progress in nanoparticle drug delivery systems has been especially associated with the immensely controllable and repeatable creation of nanoparticles as well as utilizing new biomaterials to produce nano-reservoirs. The chemico-physical characteristics of nanoparticles, like structure, dimensions, form, rigidity, and surface amendment, were directly connected to the drug release time and duration as well as delivery efficacy. For instance, the nanoparticle's size influenced the circulation time, crossing biological barriers, and organ dissemination [11–17].

Among these nanoparticle platforms, magnetic iron oxide nanoparticles (MIONs) have loomed as an extraordinary class of nanoparticles with remarkable potential for therapy and diagnosis uses, specifically cancer treatment. Holding biocompatibility, nontoxicity, small particle size, manipulation of their surface and structure, superparamagnetic, and external control and cell targeting properties, MIONs systems were broadly exploited as heat agents in magnetic hyperthermia, smart drug delivery, and magnetic resonance imaging contrast agents [18–23]. Though, MIONs owing to the robust magnetic dipole-dipole drawing power amongst nanoparticles tended to agglomerate. Polymers were extensively employed to increase the constancy and bio-inertness of MIONs [20, 21]. Chitosan (CTS) was a natural, hydrophilic, and cationic polymer with primary amine and hydroxyl groups which was suitable to alter the MIONs. The desired biological properties of this natural green polysaccharide including, low immunogenicity, biocompatibility, hydrophilicity, high biodegradability, and low toxicity made it a unique polymer for biomedical applications [24–30].

Consequently, CTS-MIONs have been used in several studies to carry the therapeutic agents and increase their therapy effects. For cancer cell targeting, the CTS-MIONs could deliver doxorubicin to Hep-G2 and MCF-7 cancer cells and enhance tumor cell toxicity

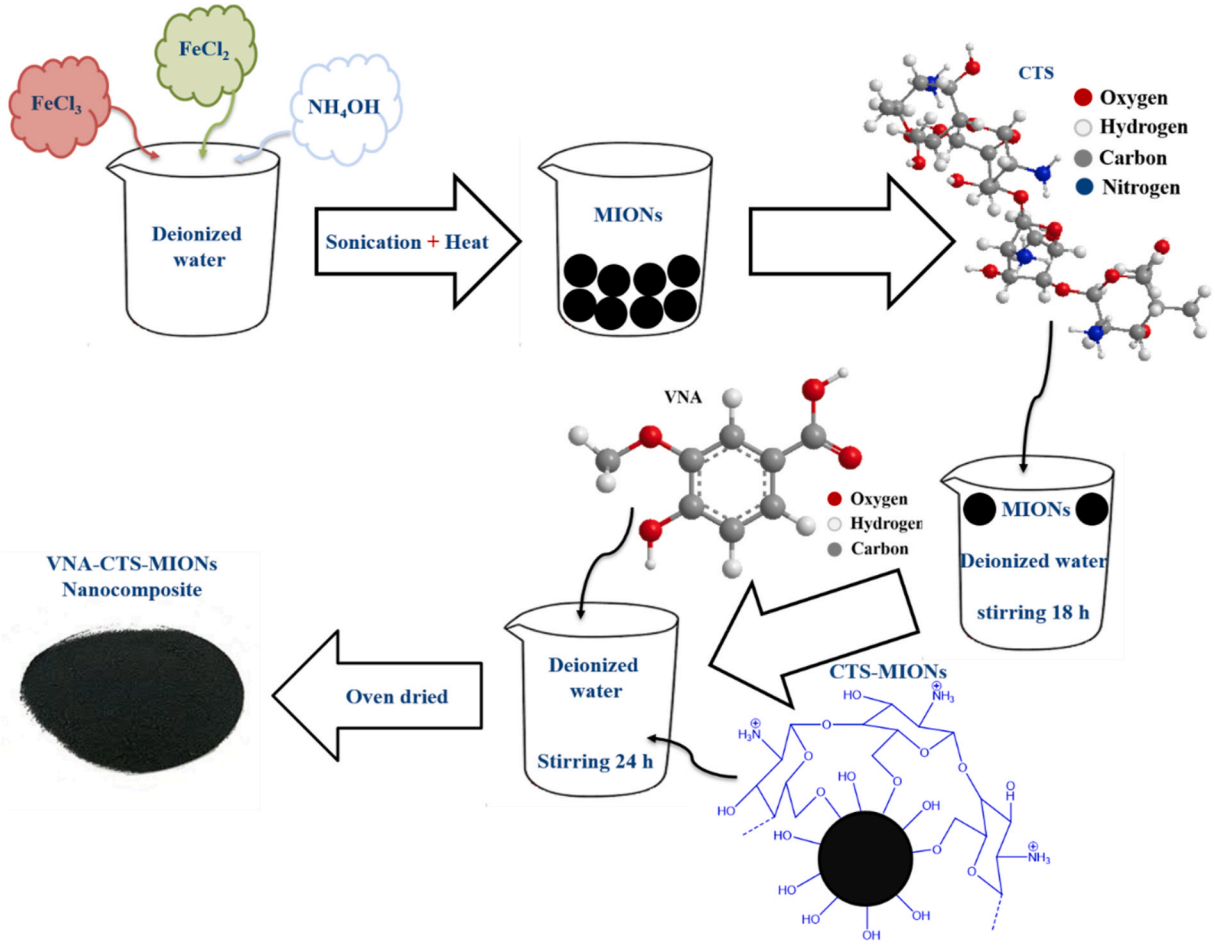

Fig. 1. Process description of MIONs, CTS-MIONs, and VNA-CTS-MIONs nanocomposite production.

[31]. Similarly, CTS-MIONs carrying phytic acid resulted in decreased tumor growth in the HT-29 cancer cell lines [32]. Also, the CTS-MIONs nanocarrier containing paclitaxel had a good suppression influence in MCF-7 cancer cells [33]. Besides, the CTS-MIONs conjugated tannic acid showed a significant antitumor effect in vitro when cervical cancer HeLa cell lines were treated [34].

Vanillic acid (4-hydroxy-3-methoxy benzoic acid, VNA) was a natural phenolic compound present in numerous natural resources including dog rose (Rosa canina), Japanese alder (Alnus japonica), Korean peroba (Paratecoma koraiensis) and China berry (Melia azedarach). It was renowned for its antioxidant, antidiabetic, cardioprotective, anti-venom, anti-inflammatory, antimicrobial, anti-sickling, hepatoprotective, and anticancer properties [35–39]. Notably, VNA had high blood-brain barrier penetration and also manifested great antitumor effect, presenting excellent potential in cancer treatment by inhibition of hypoxia-inducible factor 1 (a significant factor in tumor tolerance to micro-environmental hypoxia, angiogenesis, and tumor growth) expression caused by hypoxia in diverse human cancer cell lines. It suppressed cancer cell growth in colon, breast, lung, and prostate cancers [40–42].

However, the fast release of VNA substantiated a very short half-life of the drug and no data was on the delivery of VNA through CTS-MIONs either. Therefore, we developed VNA-CTS- MIONs nanocomposite comprising MIONs coated with CTS and VNA to achieve VNA delivery, pH-triggered VNA release, and succeeding interactive anticancer activity. The objectives of this work were to synthesize and characterize VNA-CTS-MIONs nanocomposite, release the VNA in a pH-dependent way, and attain a cell-death consequence. Accordingly, we evaluated the thermal stability, surface morphology, and particle size, as well as sustained-release property of the resulting nanocomposite. Furthermore, we investigated the effects on viability in breast cancer MDA-MB-231 cells when exposed to this nanocomposite.

2. Experimental

2.1. Materials

Chitosan (low molecular weight, deacetylation 75%–85 %) and vanillic acid of 97 % purity ($C_8H_8O_4$, with molecular weight 168.1 g mol^{-1}) were procured from Sigma-Aldrich (Saint Louis, MO, USA). Ferrous chloride tetrahydrate ($FeCl_2{\cdot}4H_2O$, 99 %) and ferric chloride hexahydrate ($FeCl_3{\cdot}6H_2O$, 99 %) were supplied from Merck KGaA, Darmstadt, Germany. Acetic acid solution 99.8 % was obtained from Hamburg Industries Inc (Hamburg, Germany) and ammonia solution (25 %) was ordered from Scharlau (Sentmenat, Barcelona, Spain).

2.2. Preparation of MIONs, CTS-MIONs, and VNA-CTS-MIONs nanocomposite

The MIONs were produced by the co-precipitation process [43]. The mixture of 2.43 g ferrous chloride tetrahydrate, 0.99 g ferric chloride hexahydrate, 80 mL deionized water, and 6 mL ammonia hydroxide was subjected to ultrasonic irradiation for 60 min. The precipitate was centrifuged and washed with deionized water (Fig. 1).

1 % acetic acid solution was used to dissolve 1 g of CTS, then added to the MIONs suspension and stirred for 18 h at room temperature. The resultant was centrifuged, washed, dried at 60 °C, and named CTS-MIONs (Fig. 1) [44].

A known amount of CTS-MIONs was added to the 2 % VNA solution (2 g VNA in 100 mL solvent). The mixture was under vigorous stirring for 24 h. The obtained precipitate was centrifuged, washed, and dried to acquire a VNA-CTS-MIONs nanocomposite (Fig. 1).

2.3. Characterization of VNA-CTS-MIONs nanocomposite

Fourier transform infrared (FTIR) spectroscopy of the samples was recorded over the range of 400–4000 cm^{-1} on a spectrophotometer (1752X, PerkinElmer, Waltham, MA, USA) with the KBr disc method. The Lake Shore 7404 vibrating sample magnetometer (Lake Shore Cryotronics, Inc., Westerville, OH, USA) was used to evaluate the magnetic properties of the materials. Thermogravimetric and differential thermogravimetric (TGA/DTG) analysis was accomplished using a Mettler Toledo instrument (Greifensee, Switzerland) in the range of 20–1000 °C with a heating rate of 10 °C/min under a nitrogen atmosphere (N_2 flow rate 50 mL/min). Powder X-ray diffraction patterns were recorded in the range of 5–70° with a Shimadzu XRD-6000 (Shimadzu Corporation, Kyoto, Japan) diffractometer using CuK_α radiation ($\lambda = 1.5418$ Å) at 30 kV and 30 mA with a dwell time of 4° per minute. The morphology, middle particle size, and size distribution of the samples were observed by a transmission electron microscope (Hitachi H-7100, Tokyo, Japan) at an accelerating voltage of 80 and 200 kV. A Shimadzu 1650 series UV–vis spectrophotometer (Shimadzu, Tokyo, Japan) was used to investigate the release of VNA from VNA-CTS-MIONs.

2.4. Loading and release of VNA from the VNA-CTS-MIONs nanocomposite

The loading percentage of VNA loading in the VNA-CTS-MIONs nanocomposite was found by UV–Vis spectrophotometer (Shimadzu 1650 series, Tokyo, Japan) and equation of calibration curve. VNA-CTS-MIONs (5 mg) was dissolved in concentrated HCl/HNO_3 and the VNA was released 100 % from VNA-CTS-MIONs. The released quantity of VNA was determined by UV–Vis spectrophotometer using VNA absorbance at 247 nm and calibration curves. VNA release from VNA-CTS-MIONs was measured at ambient temperature via a phosphate-buffered saline solution (PBS) at pH 5 and 7.4. About 85 mg of the VNA-CTS-MIONs was appended to 500 mL of the phosphate-buffered solution. The released quantity of VNA was determined using a UV–Vis spectrophotometer at $\lambda_{max} = 247$ nm. The release rate of VNA from VNA-CTS-MIONs was compared with that from a physical mixture that comprised CTS-MIONs nanovehicle and VNA.

2.5. Collection and maintenance of cells

The MDA-MB-231 breast cancer cells were grown in a DMEM medium with FBS (10 %) using 5 % CO_2 provided incubator. Followed by the cells reaching 80 % confluency, they were obtained by trypsinization and utilized for further cytotoxicity and fluorescent staining assays.

2.6. MTT assay

The cytotoxicity of VNA-CTS-MIONs on the breast cancer cells were investigated by MTT assay. The 96-well plate was used to grow the cells and exposed to various dosages of VNA-CTS-MIONs (2.5, 5, 7.5, 10, 12.5, and 15 μg/mL) for 24 h. After the completion of the treatment period, MTT reagent (20 μL) was added to each well along with DMEM (100 μL) for 4 h. After that, the developed formazan depositions were dissolved by adding the 100 μL DMSO into the well, and finally absorbance was assessed using a microplate reader at 570 nm.

2.7. Dual staining

The apoptosis level in the control and VNA-CTS-MIONs-exposed MDA-MB-231 cells were determined using a dual staining technique. Briefly, cells were cultivated on a 24-wellplate and then cells were treated with the 7.5 μg/mL of VNA-CTS-MIONs or 2 μg of doxorubicin (DOX, standard drug) for 24 h. After the completion of treatments, an AO/EB fluorescent stain (100 μg/mL) at 1:1 ratio was mixed with the cells for 5 min to stain the cells. The stained cells were examined using a fluorescence microscope to investigate the developed fluorescence.

2.8. DCFH-DA staining

The ROS production level in the untreated and VNA-CTS-MIONs nanocomposite-exposed cells were examined by the DCFH-DA staining technique. The breast cancer cells were cultured and then treated with 7.5 μg/mL of VNA-CTS-MIONs nanocomposite or 2 μg DOX for 24 h. Later in the treatment period, 10 μL DCFH-DA was mixed in the cells for 10 min to stain the cells. Finally, the intensity of the formed fluorescence was investigated using a fluorescence microscope to measure the endogenous ROS level.

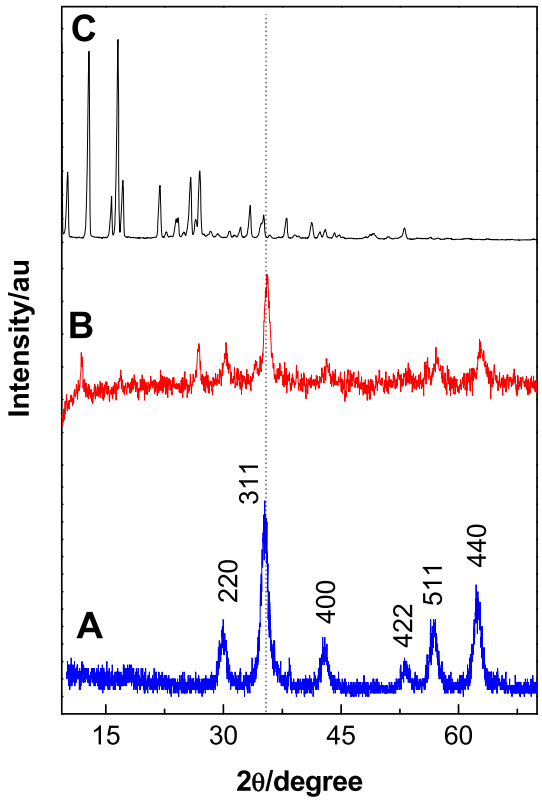

Fig. 2. XRD spectra of MIONs (A), VNA-CTS-MIONs nanocomposite (B), and VNA (C).

3. Results and discussion

3.1. XRD analysis

The XRD spectra of synthesized MIONs, VNA-CTS-MIONs nanocomposite, and free VNA were displayed in Fig. 2 (A-C). Fig. 2A indicated six characteristic peaks for MIONs at 2θ values of 30.1°, 35.4°, 43.1°, 53.5°, 57.8°, and 62.3° which corresponded to the 220, 311, 400, 422, 511, and 440 crystallographic planes of the inverse spinel MIONs crystal [45,46]. Additionally, these peaks were observed for the VNA-CTS-MIONs nanocomposite in Fig. 2B that exhibited the coating process did not alter the crystalline network of MIONs [33,47]. What is more, the average crystallite size (D) of MIONs could be determined by the Debye-Scherrer equation, $D = K\lambda/\beta\cos\theta$ [48,49] where, K was a constant, λ was wavelength, β was the peak width of half-maximum, and θ was the diffraction angle. The middle diameter of MIONs was calculated at around 9 nm.

3.2. FTIR analysis

The successful formation of MIONs, CTS-MIONs, and VNA-CTS-MIONs nanocomposite was substantiated by FTIR analyses and the spectra of MIONs, CTS-MIONs, VNA-CTS-MIONs nanocomposite, and VNA were shown in Fig. 3(A-D). The broad characteristic bands were observed at 3415 cm^{-1}, 3418 cm^{-1}, and 3406 cm^{-1} in Fig. 3A, B, and C were ascribed to OH stretching vibration. The characteristic peak of Fe–O stretching in Fe_3O_4 was detected at 569 cm^{-1} and 565 cm^{-1} in FTIR spectra of MIONs (Fig. 3A) and CS-MIONs (Fig. 3B), respectively, and it appeared at 579 cm^{-1} in FTIR spectra of VNA-CTS-MIONs nanocomposite that proved the presence of MIONs [50]. Three absorption bands at 1624 cm^{-1}, 1384 cm^{-1}, and 1062 cm^{-1} were observed in Fig. 3B that could be attributed to N–H bending vibration, –C–O stretching of the alcohol group, and glycosidic bond stretching vibration, respectively in CTS [51–53]. These results confirmed the successful coating of MIONs by CTS biopolymer. The FTIR spectra of VNA in Fig. 3D, demonstrated numerous strong, sharp charcteristic peaks that were caused by various functional groups present in VNA including phenol, carboxylic acid and, ether groups. The carbonyl group of the carboxylic acid functional group recorded a band at 1679 cm^{-1} and OH stretching vibration appeared at 3482 cm^{-1}. The peaks at 1597 cm^{-1}, 1521 cm^{-1}, and 1471 cm^{-1} were attributable to the CH stretching of the aromatic ring while the peaks at 1432 cm^{-1} and 1382 cm^{-1} were related to the CH_3 bending and ring stretching. CO (COH) stretching vibration of the carboxylic acid functional group was detected at 1297 cm^{-1}, CO (C–*O*–CH3) stretching at 1237 cm^{-1} and 1110 cm^{-1}, and CO stretching of the phenol functional group (Ar-OH) at 1205 cm^{-1}. The peak at 917 cm^{-1} was ascribed to the OH bending of the COOH functional group and CH bending vibrations [35,37,54]. The disappearance of typical peaks of carboxylic acid functional group

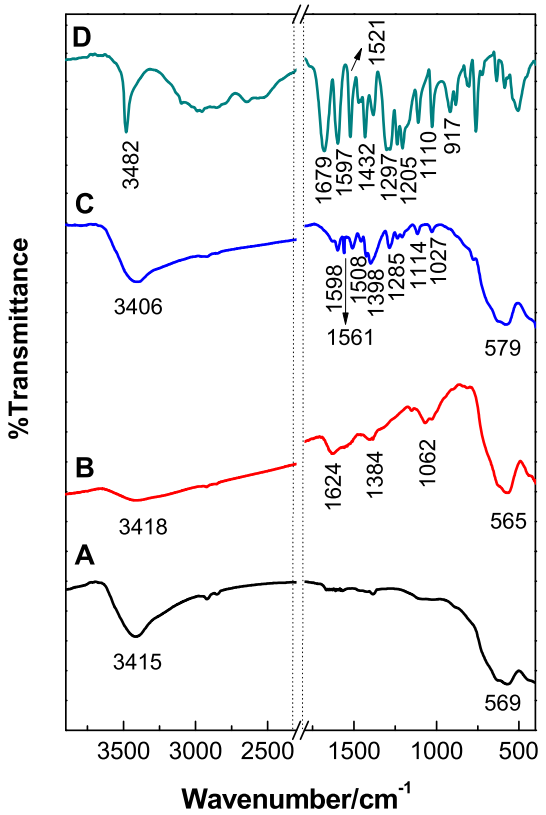

Fig. 3. FTIR spectra of MIONs (A), CTS-MIONs (B), VNA-CTS-MIONs nanocomposite (C), and VNA (D).

at 1679 cm^{-1} and 917 cm^{-1} and observation of stretching vibrations at 1598 cm^{-1} and 1398 cm^{-1} due to the new amide linkage besides the bending vibration of N–H at 1561 cm^{-1} in FTIR spectra of VNA-CTS-MIONs nanocomposite (Fig. 3C) revealed that VNA was successfully loaded on CTS-MIONs. The CH stretching vibrations of the aromatic ring were detected at 1508 cm^{-1} and 1456 cm^{-1} and the peaks at 1285 cm^{-1}, 1114 cm^{-1}, and 1027 cm^{-1} were associated with the CO groups (Fig. 3C).

The solubility of CTS biopolymer in acetic acid resulted in the creation of NH^{+} ^{3} in CTS structure and the findings supported the interaction of VNA with these amino groups of CTS via hydrogen bonds as well as CTS interaction with MIONs through glycosidic bonds (Fig. 4).

3.3. Thermal analysis

The TGA/DTG curves of VNA, MIONs, and VNA-CTS-MIONs nanocomposite were exposed in Fig. 5. The TGA/DTG curve of VNA (Fig. 5A) disclosed one main thermal event at 217 °C with a mass loss of 98.9 % ascribable to the decomposition of VNA. For MIONs Fig. 5B demonstrated two weight loss steps at 47 °C and 120 °C which could be assigned to the removal of the surface hydroxyl groups and residual water [55,56]. Fig. 5C contained two stages of mass loss for VNA-CTS-MIONs nanocomposite at 304 °C and 633 °C. These stages were ascribed to the decomposition of VNA and CTS biopolymer with 13.1 % and 6.4 % of weight loss. The temperature region in VNA-CTS-MIONs nanocomposite was higher than for free VNA which verified the coating procedure enhanced the thermal constancy of VNA.

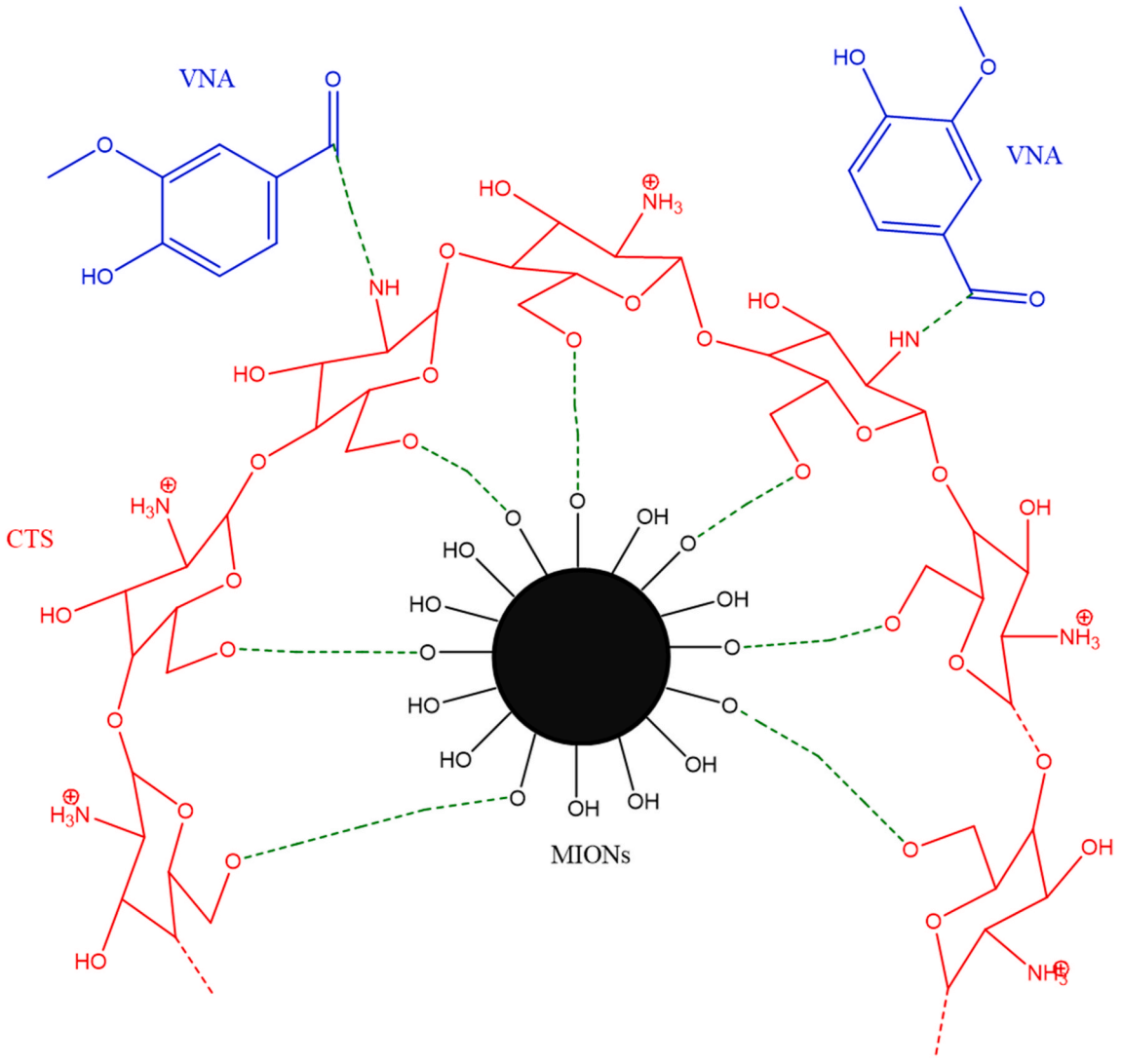

Fig. 4. Scheme illustrating of the interaction amid MIONs, CTS, and VNA in the VNA-CTS-MIONs.

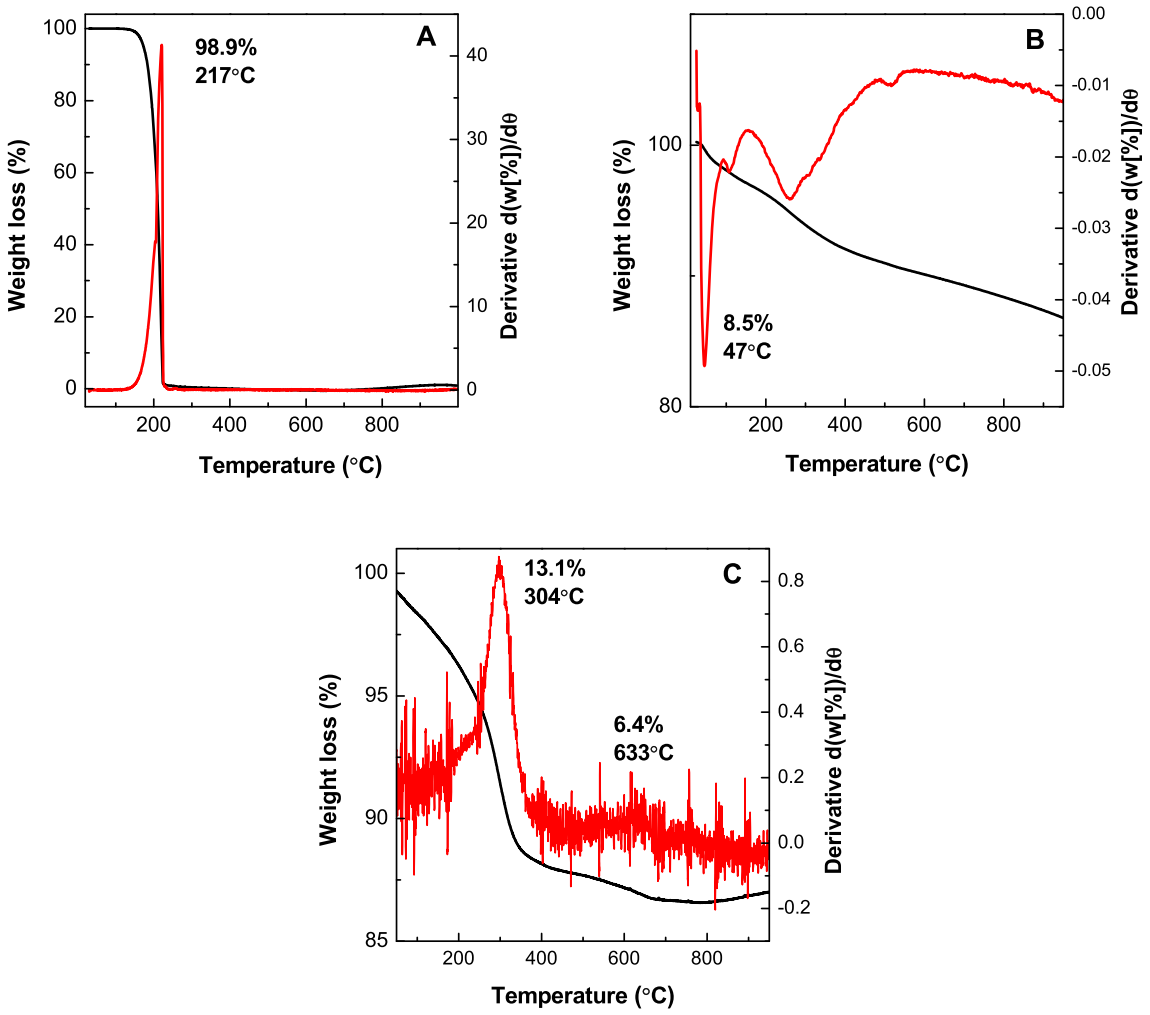

Fig. 5. TGA/DTG curves of VNA (A), MIONs (B), and VNA-CTS-MIONs (C).

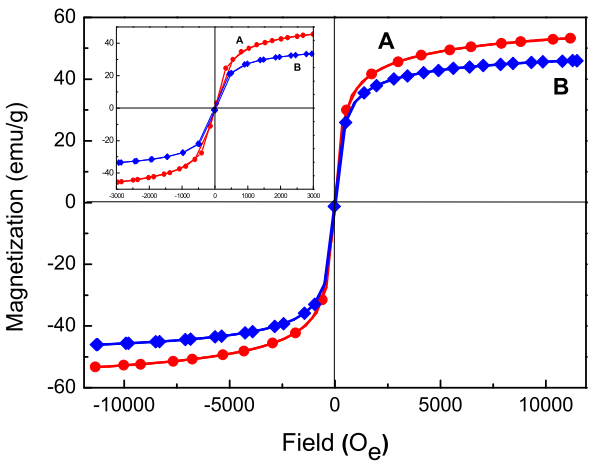

Fig. 6. Magnetization curves of MIONs (A) and VNA-CTS-MIONs nanocomposite (B) measured at room temperature. The inset shows the magnetic behaviour in low magnetic fields.

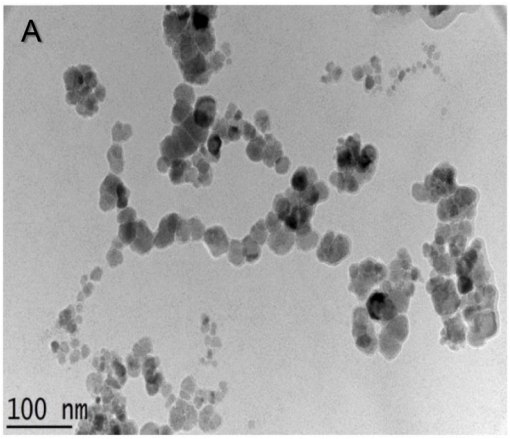

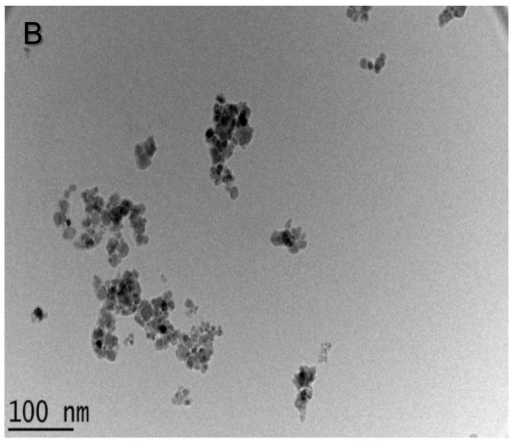

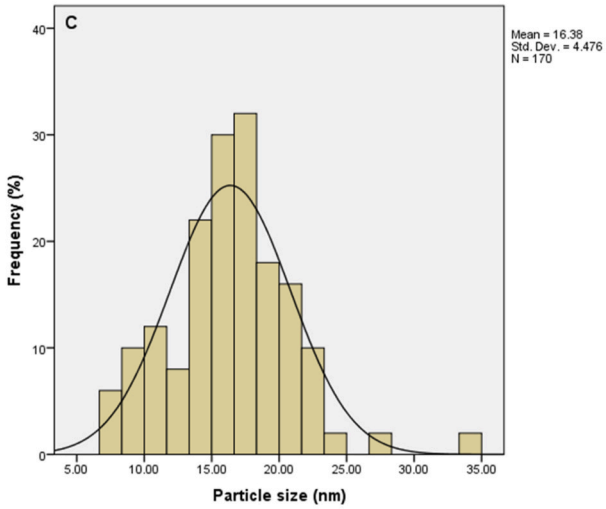

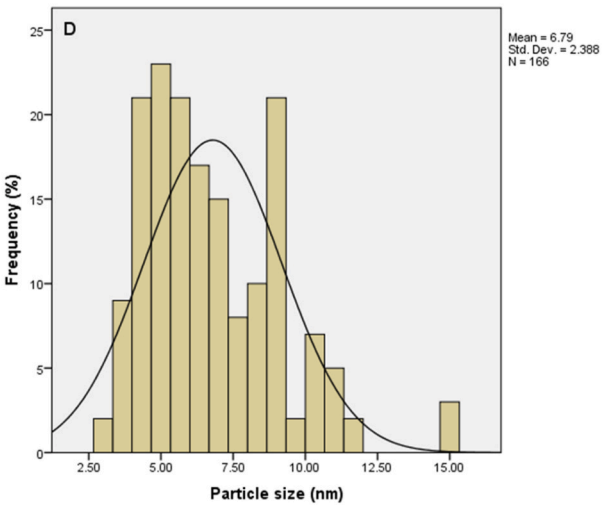

(caption on next page)

Fig. 7. TEM images for MIONs (A) and VNA-CTS-MIONs (B), and particle size dispersal of MIONs (C) and VNA-CTS-MIONs (D).

3.4. Magnetic properties

The magnetic properties of MIONs and VNA-CTS-MIONs nanocomposite were revealed in Fig. 6 (A and B). The MIONs' magnetization curve (Fig. 6A) exhibited saturation magnetization (M_s) of about 53.3 emu/g compared with 45.7 emu/g for VNA-CTS-MIONs nanocomposite (Fig. 6B). Both samples manifested zero remnance and coercivity which offered superparamagnetic properties in MIONs and VNA-CTS-MIONs nanocomposite. The lower magnetization of the VNA-CTS-MIONs nanocomposite corroborated that CTS biopolymer bound to MIONs and anticancer agent, VNA was loaded on the surface of the CTS-MIONs nanovector.

3.5. Determination of middle size and size distribution features

Transmission electron microscopy (TEM) micrographs and size distribution of MIONs and VNA-CTS-MIONs were shown in Fig. 7. It could be seen from images (Fig. 7A and B) that particles in both samples; MIONs and VNA-CTS-MIONs were nanosized with nearly spherical shapes. The middle diameter of MIONs was about 16 ± 5 nm (Fig. 7A and C) compared with 6 ± 4 nm for VNA-CTS-MIONs nanocomposite (Fig. 7B and D). The smaller particle size of the nanocomposite might be due to the vigorous stirring for a long time after the addition of the CTS and VNA, as well as the same consequences were reported by the literature [32,57,58].

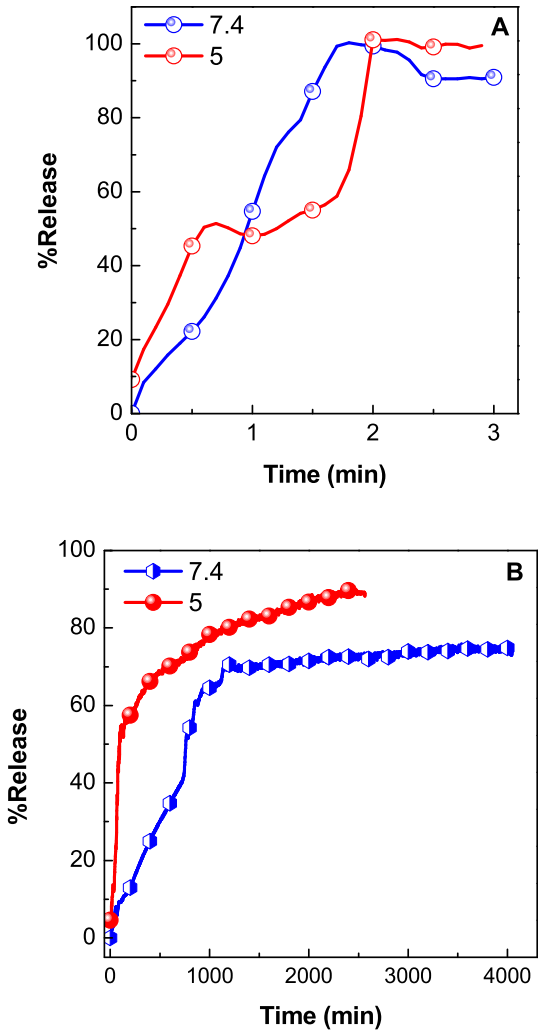

Fig. 8. Release curves of a physical mixture of VNA with CTS-MIONs at pH 7.4 and pH 5 (A) and release curves of VNA from VNA-CTS-MIONs at pH 7.4 and pH 5 (B).

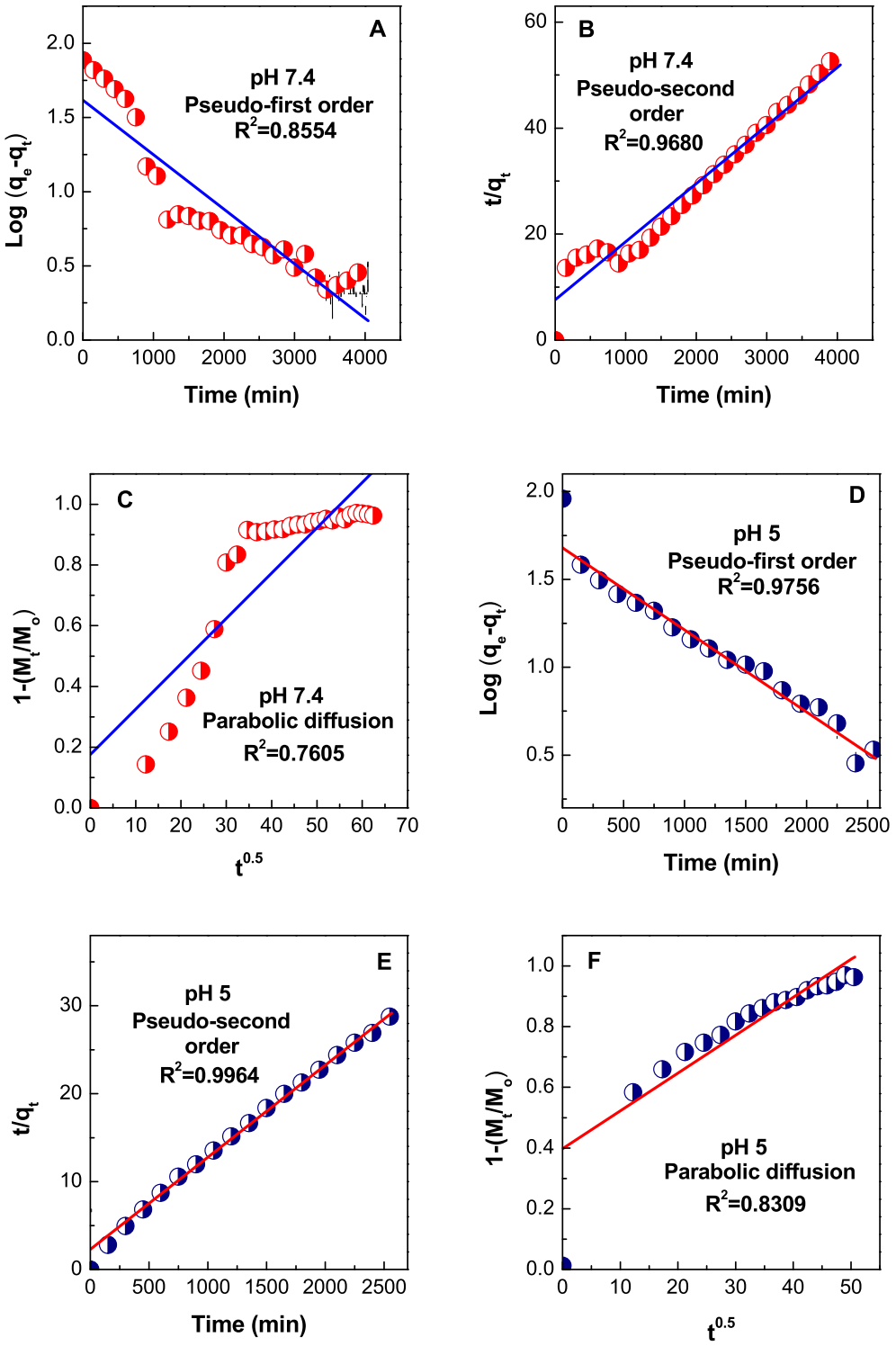

Fig. 9. Suiting of the data for VNA release from VNA-CTS-MIONs in diverse solutions to the first-order, pseudo-second order kinetics and parabolic diffusion model for pH 7.4 (A–C) and pH 5 (D–F).

3.6. In vitro release study of VNA from VNA-CTS-MIONs nanocomposite

To substantiate pH-responsive controlled release of anticancer active agent, VNA from VNA-CTS-MIONs nanocomposite, in vitro release of VNA from obtained nanocomposite were performed in phosphate-buffered solution (PBS) with pH 7.4 (blood) and 5 (intracellular environment), as presented in Fig. 8. The pH values were chosen by holding in view of the physiological pH of normal tissue and blood (pH 7.4) and intracellular pH of cancer tissue (pH 5). The release patterns for the physical mixture of VNA in pH 5 and pH 7.4 PBS were indicated in Fig. 8A. It turned up that VNA was rapidly released from the physical mixture and VNA release was accomplished in 2 min at pH 5 and 7.4. This was a consequence of the low electrostatic attraction between VNA and CTS-MIONs. Fig. 8B exhibited the release rate of VNA at pH 5 and 7.4 PBS and showed that the VNA release profiles from VNA-CTS-MIONs nanocomposite were sustained and depended on pH in compared to the VNA release from the physical mixture in pH 5 and pH 7.4 PBS. Triggered by the intracellular pH of cancer tissue (pH 5), VNA-CTS-MIONs nanocomposite could cause almost fast release of VNA under an acidic condition compared to pH 7.4 and induced CTS- MIONs nanocarrier dismantlement along with VNA release. The release rate at pH 7.4 is substantially less than that at pH 5. The maximum percent release of VNA from the VNA-CTS-MIONs reached 89 % and 74 % in about 2354 and 4046 min when subjected to pH 5 and 7.4, respectively. The dissimilar release rates at pH 5 and 7.4 PBS were presumably owing to the various release mechanisms of VNA from the VNA-CTS-MIONs nanocomposite. The VNA-CTS-MIONs nanocomposite was more durable at pH 7.4, and the VNA release from VNA-CTS-MIONs nanocomposite might occur via an anion substitution process between the VNA anions and phosphate anions in the PBS [33,59–62]. The sustained and pH-dependent-ascertained trend in the release profile of VNA from VNA-CTS-MIONs nanocomposite can be elucidated by conceiving the controlled release and pH-responsive physicochemical characteristics of the CTS-MIONs nano-vector which escalates drug half-life period and enhances therapeutic response in cancer therapy.

The data of the in vitro release mechanism of VNA from CTS-MIONs nano-vehicle gave diverse beneficial structural and kinetic parameters for its in vivo usage in interior cellular environments. Thus, we explored the release profiles of VNA-CTS-MIONs nanocomposite with three kinetic models; pseudo-first-order (equation (1)) [63,64], pseudo-second-order (equation (2)) [65], and parabolic diffusion (equation (3)) [66].

$$\ln(q_e\text{-}q_t) = \ln q_e - k_1 t \quad (1)$$

$$t/q_t = 1/k_2 q_e^2 + t/q_e \quad (2)$$

$$(1\text{-}M_t/M_o)/t = k_3 t^{-0.5} + b \quad (3)$$

The q_e and q_t were the equilibrium release amount and the release amount at time t, respectively, k was the invariant of the related release rate, and M_0 and M_t showed the remained VNA amount in the VNA-CTS-MIONs at release times 0 and t, respectively.

Suiting the data for the release of anticancer agent, VNA to these kinetic models, it emerged that the pseudo-second-order kinetic model described satisfactorily the release of VNA from VNA-CTS-MIONs at both pH levels (Fig. 9A–F and Table 1). These results were very akin to the release kinetic investigation of the protocatechuic acid and chlorogenic acid from Zn/Al-layered double hydroxide [67,68].

The correlation coefficient (R^2) and k_2 values were 0.9680 and 1.58×10^{-5} L/mg.min for pH 7.4 (Fig. 9B and Table 1), compared to 0.9964 and 4.79×10^{-5} L/mg.min for pH 5 (Fig. 9E and Table 1), respectively.

3.7. Effect of VNA-CTS-MIONs nanocomposite on the breast cancer cell viability

The findings of the VNA release test proposed to investigate the cellular intake and cytotoxicity of VNA-CTS-MIONs. In the present work, the anticancer effects of VNA-CTS-MIONs were assessed against MDA-MB-231 cells. The MTT test was conducted to assess the VNA-CTS-MIONs-treated cell growth (Fig. 10). The exposure of several dosages of the VNA-CTS-MIONs (2.5–15 μg/mL) remarkably diminished the cell growth in dosage-dependently when compared to control. The 7.5 μg/mL of VNA-CTS-MIONs treatment resulted in a lower than 50 % reduction in MDA-MB-231 cell viability; consequently, 7.5 μg/mL was selected as an IC_{50} concentration for additional studies.

3.8. Effect of VNA-CTS-MIONs on the ROS accumulation in the MDA-MB-231 cells

The nanoparticles catalyzed the generation of ROS with the help of oxygen species, which could produce oxidative stress in several tumor cells. When oxidant and antioxidant levels were balanced, ROS-mediated oxidative stress could regulate many physiological

Table 1
Correlation coefficient (R^2), rate constants (k_2), and half time ($t_{1/2}$) values gained by suiting the data of the release of VNA from VNA-CTS-MIONs in PBS at pH 5 and 7.4.

Aqeous solution	saturation release (%)	R^2			Pseudo-second order	
		Pseudo- first order	Pseudo- second order	Parabolic diffusion	Rate constant, K_2 (L/mg.min)	$t_{1/2}$ (min)
pH 7.4	74	0.8554	0. 9680	0.7605	1.58×10^{-5}	693
pH 5	89	0.9756	0.9964	0.8309	4.79×10^{-5}	218

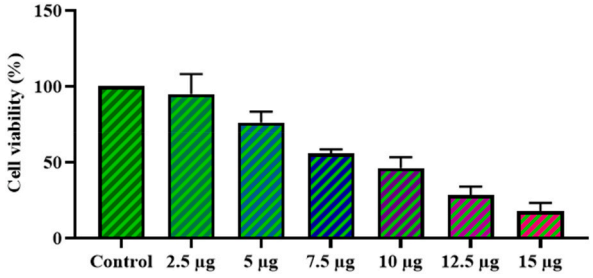

Fig. 10. Effect of VNA-CTS-MIONs nanocomposite on the MDA-MB-231 cell growth. The treatment with the diverse concentrations of VNA-CTS-MIONs (2.5–15 µg) was effectively diminished the MDA-MB-231 cell viability. Values are depicted as mean ± SD of triplicate assays.

activities, including cell growth, apoptosis, and necrosis. Chemotherapeutic drugs, cytotoxic agents, and nanoparticles all contributed to an equilibrium between oxidants and antioxidants in cancer cells, thereby facilitating cell death [69].

The level of ROS production in the untreated and VNA-CTS-MIONs nanocomposite-exposed MDA-MB-231 cells were investigated by the DCFH-DA fluorescent staining assay. As per the outcomes illustrated in Fig. 11, the treatment with 7.5 µg/mL VNA-CTS-MIONs nanocomposite resulted in increased green fluorescence, which correlated to the upsurge in ROS buildup in MDA-MB-231 cells than the control. Therefore, it was proved that the VNA-CTS-MIONs nanocomposite boosted endogenous ROS accumulation, which could promote apoptosis in MDA-MB-231 cells. It was well known that enhanced ROS production promoted mitochondria-dependent cell death pathways [70].

3.9. Effect of VNA-CTS-MIONs nanocomposite on the apoptosis level in breast cancer cells

Apoptosis, a type of programmed cell death, was essential for the proper development and maintenance of tissues. Deregulation of apoptosis was linked to both the development of cancer and resistance to treatment. Defects in cancer suppressor genes led to cancer development by disrupting apoptotic signaling [71]. Membrane disruption, growth arrest, cytoplasmic reduction, and cell aggregation were all potential precipitating factors in apoptosis. The apoptosis in the breast cancer cells was investigated by dual staining technique and the outcomes were presented in Fig. 12. The untreated cells revealed increased green fluorescence without apoptosis. However, the treatment with the 7.5 µg/mL VNA-CTS-MIONs nanocomposite substantially increased the orange/yellow fluorescence, which indicated the increased presence of apoptosis in the breast cancer cells. The apoptosis-triggering potentials of the VNA-CTS-MIONs were supported by the outcomes of DOX treatment that also elevated apoptosis in the breast cancer cells. The anticancer effectiveness of medicines was largely thought to be driven by apoptosis induction in tumor cells [72]. Cancer cells experiencing apoptosis exhibited a wide variety of morphological alterations, including cellular shrinkage, membrane blebbing, and nuclear fragmentation [73]. These morphological changes were also seen in the MDA-MB-231 cells, which were exposed to the VNA-CTS-MIONs nanocomposite.

4. Conclusions

Extended-release, structurally robust, and pH-sensitive nanocarrier was developed for tumor-specific delivery of an anticancer agent. This study showed that the new nanocomposite, VNA-CTS-MIONs containing a novel CTS-MIONs nano-reservoir and anticancer agent, VNA has been successfully synthesized. The binding of the CTS on the MION surface was asserted by FTIR, similar to the loaded VNA. The VNA loading in the nanohybrid was 11.8 % and release of VNA from fabricated nanocomposite was pH-depended and in a prolonged way with total equilibrium release of 74 % in 4046 min and 89 % in 2354 min at pH 7.4 and 5 PBS, respectively. The pseudo-second-order kinetic model was the perfect match for VNA release from the nanocomposite and the TEM size image of MIONs and VNA-CTS-MIONs nanocomposite was about 16 and 6 nm, respectively. The TGA/DTG thermograms signified that the thermal constancy of VNA enhanced in the nanocomposite and CTS-MIONs nano-carrier enhanced thermal stability of VNA and saturation magnetizations of 53.3 was also observed for the superparamagnet nanocomposite. The VNA-CTS-MIONs nanocomposite treatment effectively reduced the viability and promoted ROS production and apoptosis in the MDA-MB-231 cells. Therefore, it can be a prospective anticancer agent for the cure of breast cancer.

Additional information

No additional information is available for this paper.

Ethics statement

Not applicable.

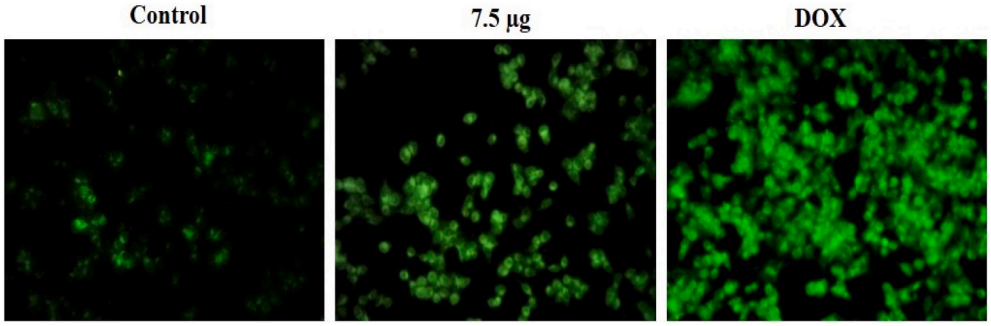

Fig. 11. Effect of VNA-CTS-MIONs nanocomposite on the ROS accumulation in the MDA-MB-231 cells. The VNA-CTS-MIONs nanocomposite and DOX treatment remarkably boosted the ROS buildup in the MDA-MB-231 cells.

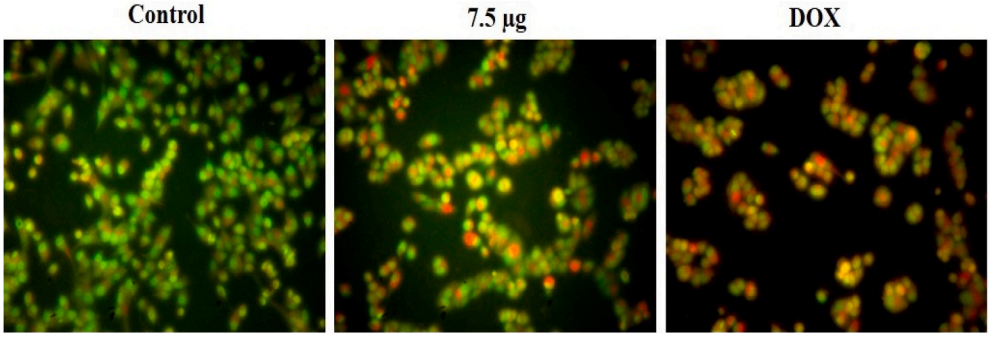

Fig. 12. Effect of VNA-CTS-MIONs on the apoptosis in breast cancer cells. The treatment with VNA-CTS-MIONs and DOX led to the high yellow/orange fluorescence that proves the increased occurrence of early and late apoptosis, respectively in the MDA-MB-231 cells. (For interpretation of the references to colour in this figure legend, the reader is referred to the Web version of this article.)

Data availability statement

Data will be made available on request.

CRediT authorship contribution statement

Farahnaz Barahuie: Writing – review & editing, Writing – original draft, Visualization, Validation, Software, Methodology, Investigation, Formal analysis, Data curation, Conceptualization. **Dena Dorniani:** Methodology, Formal analysis. **Bullo Saifullah:** Methodology, Formal analysis. **Palanisamy Arulselvan:** Writing – original draft, Validation, Methodology, Investigation, Formal analysis, Data curation. **Mohd Zobir Hussein:** Supervision, Project administration, Funding acquisition. **Ravindran Jaganathan:** Formal analysis. **Fawzi Mohamed Amin El-Fagaih:** Formal analysis. **Ariyati Retno Pratiwi:** Formal analysis.

Declaration of competing interest

The authors declare that they have no known competing financial interests or personal relationships that could have appeared to influence the work reported in this paper.

References

[1] Yanyu Zhang, Xiaoxi Huang, Xingxing Yu, Wei He, Kamila Czene, Haomin Yang, Hematological and biochemical markers influencing breast cancerrisk and mortality: prospective cohort study in the UK Biobank bymulti-state models, Breast 73 (2024) 103603.
[2] J. Dewangan, D. Tandon, S. Srivastava, A.K. Verma, A. Yapuri, S.K. Rath, Novel combination of salinomycin and resveratrol synergistically enhances the antiproliferative and pro-apoptotic effects on human breast cancer cells, Apoptosis 22 (2017) 1246–1259.
[3] J.S. Passos, V.F.M.C. Dartora, G.C. Salata, I.D. Malago, L.B. Lopes, Contributions of nanotechnology to the intraductal drug delivery for local treatment and prevention of breast cancer, Int. J. Pharm. 635 (2023) 122681.
[4] K. Elumalai, S. Srinivasan, A. Shanmugam, Review of the efficacy of nanoparticle-based drug delivery systems for cancer treatment, Biomed, Technol. 5 (2024) 109–122.
[5] X. Luo, K. Jia, J. Xing, J. Yi, The utilization of nanotechnology in the female reproductive system and related disorders, Heliyon 10 (3) (2024) e25477.
[6] Y.-J. Xie, M. Huang, D. Li, J.-C. Hou, H.-H. Liang, A.A. Nasim, J.-M. Huang, C. Xie, E.L.-H. Leung, X.-X. Fan, Bacteria-based nanodrug for anticancer therapy, Pharmacol. Res. 182 (2022) 106282.

[7] M. Arif, A. Fazal Nawaz, S.U. khan, H. Mueen, F. Rashid, H.A. Hemeg, A. Rauf, Nanotechnology-based radiation therapy to cure cancer and the challenges in its clinical applications, Heliyon 9 (2023) e17252.
[8] S.A. Jasim, M.S. Al-Lami, Aa J, A.H. Shather, a.k. Aldhalmi, A.G. Taki, B.A. Ahmed, M.M. Al-Hamdani, S.K. Saraswat, Nanostructures of boron nitride: a promising nanocarrier for anti-cancer drug delivery, Micro Nanostructures 185 (2024) 207708.
[9] S. Guo, J. Wang, Q. Wang, J. Wang, S. Qin, W. Li, Advances in peptide-based drug delivery systems, Heliyon 10 (4) (2024) e26009.
[10] J.-J. Zhang, Q.J. Xu, Y. Zhang, Q. Zhou, R. Lv, Z. Chen, W. He, Recent advances in nanocarriers for clinical platinum(II) anticancer drugs, Coord. Chem. Rev. 505 (2024) 215676.
[11] K. Brindhadevi, H. Al-Garalleh, A. Alalawi, E. Al-Sarayreh, A. Pugazhendhi, Carbon nanomaterials: Types, synthesis strategies and their application as drug delivery system for cancer therapy, Biochem. Eng. J. 192 (2023) 108828.
[12] S. Sadiq, S. Khan, I. Khan, A. Khan, M. Humayun, P. Wu, M. Usman, A. Khan, A.F. Alanazi, M. Bououdina, A critical review on metal-organic frameworks (MOFs) based nanomaterials for biomedical applications: Designing, recent trends, challenges, and prospects, Heliyon 10 (3) (2024) e25521.
[13] P. Sharma, K. Patnala, N. Sah, V.K. Deb, N. Gopal, N. Chauhan, R. Chandra, U. Jain, Revamping precision treatment with nanoparticles envisaging effective drug delivery systems for ovarian cancer, Process Biochem. 138 (2024) 33–46.
[14] S. Ajith, F. Almomani, A. Elhissi, G.A. Husseini, Nanoparticle-based materials in anticancer drug delivery: Current and future prospects, Heliyon 9 (11) (2023) e21227.
[15] V. Janakiraman, M. J, S.K. B, T. M, P. Ramasamy, K. Kannan, I. Ahmad, M.J. Ansari, S. Pitchiah, Applications of fungal based nanoparticles in cancer therapy- A review, Process Biochem. 140 (2024) 10–18.
[16] P. Singh, P.K. Katkar, T. Walski, R.A. Bohara, Three in-one fenestrated approaches of yolk-shell, silver-silica nanoparticles: a comparative study of antibacterial, antifungal and anti-cancerous applications, Heliyon 9 (2023) e18034.
[17] H.W. Chan, S. Chow, X. Zhang, P.C.L. Kwok, S.F. Chow, Role of particle size in translational research of nanomedicines for successful drug delivery: Discrepancies and inadequacies, J. Pharm. Sci. 112 (2023) 2371–2384.
[18] F. Razmimanesh, G. Sodeifian, Evaluation of a temperature-responsive magnetotocosome as a magnetic targeting drug delivery system for sorafenib tosylate anticancer drug, Heliyon 9 (2023) e21794.
[19] M. Prakash, M.N. Chandraprabha, R.H. Krishna, H. Satish, S.G. Kumar, Iron oxide nanoparticles for inflammatory bowel disease: recent advances in diagnosis and targeted drug therapy, Appl. Surf. Sci. Adv. 19 (2024) 100540.
[20] C. Turrina, A. Klassen, D. Milani, D.M.R. Gonzalez, G. Ledinski, D. Auer, B. Sartori, G. Cvirn, P. Mela, S. Berensmeier, S.P. Schwaminger, Superparamagnetic iron oxide nanoparticles for their application in the human body: influence of the surface, Heliyon 9 (6) (2023) e16487.
[21] M. Swietek, I. Markova, H. Malinska, M. Huttl, D. Miklankova, K. Cerna, R. Konefal, D. Horak, Tannic acid- and *N*-acetylcysteine-chitosan-modified magnetic nanoparticles reduce hepatic oxidative stress in prediabetic rats, Colloids Surf. B Biointerfaces 235 (2024) 113791.
[22] T.A. Alkinani, F.A. Bajgiran, M. Rezaei, A.M. Maivan, F.J. Golrokh, M. Bejarbaneh, S.R. Mojdehi, S. Gorji, R. Ghasemian, M.D.J.P. Sarai, F. Akbari, S. Dehghan, F. Mirzaee, N.H. Abdulrahman, A. Salehzadeh, Evaluation the cytotoxic effect of Fe_3O_4@Glu-Gingerol on lung adenocarcinoma cell line (A549) with biological mechanisms, Heliyon 10 (1) (2024) e23419.
[23] B.S. Dash, Y.-J. Lu, Y.-S. Huang, J.-P. Chen, Chitosan-coated magnetic graphene oxide for targeted delivery of doxorubicin as a nanomedicine approach to treat glioblastoma, Int. J. Biol. Macromol. 260 (2024) 129401.
[24] Y. Herdiana, N. Wathoni, S. Shamsuddin, M. Muchtaridi, Drug release study of the chitosan-based nanoparticles, Heliyon 8 (2022) e08674.
[25] A.K. Sahdev, C.J. Raorane, D. Shastri, V. Raj, A. Singh, S.C. Kim, Update on modified chitosan frameworks and their applications for food, wastewater, toxic heavy metals, dyes treatment and cancer drug delivery, J. Environ. Chem. Eng. 10 (2022) 108656.
[26] Y. Zaiki, A. Iskandar, T.W. Wong, Functionalized chitosan for cancer nano drug delivery, Biotechnol. Adv. 67 (2023) 108200.
[27] S. Javed, G. Abbas, S. Shah, A. Rasul, M. Irfan, A. Saleem, K.M. Hosny, S.M. Bukhary, A.Y. Safhi, F.Y. Sabei, M.A. Majrashi, H.M. Alkhalidi, M. Alissa, S.M. Khan, M. Hanif, Tobramycin-loaded nanoparticles of thiolated chitosan for ocular drug delivery: Preparation, mucoadhesion and pharmacokinetic evaluation, Heliyon 9 (9) (2023) e19877.
[28] M.H. Elkomy, A.A. Ali, H.M. Eid, Chitosan on the surface of nanoparticles for enhanced drug delivery: a comprehensive review, J. Contr. Release 351 (2022) 923–940.
[29] M. Kurakula, S. Gorityala, K. Moharir, Recent trends in design and evaluation of chitosan-based colon targeted drug delivery systems: Update 2020, J. Drug Deliv. Sci. Technol. 64 (2021) 102579.
[30] A. Rafiee, N. Mozafari, N. Fekri, M. Memarpour, A. Azadi, Preparation and characterization of a nanohydroxyapatite and sodium fluoride loaded chitosan-based *in situ* forming gel for enamel biomineralization, Heliyon 10 (2024) e24217.
[31] M.Y. Nassar, H.I. El-Salhy, W.H. El-Shiwiny, G. Abdelaziz, R. El-Shiekh, Composite nanoarchitectonics of magnetic silicon dioxide-modified chitosan for doxorubicin delivery and in vitro cytotoxicity assay, J. Inorg. Organomet. Polym. Mater. 33 (2023) 237–253.
[32] F. Barahuie, D. Dorniani, B. Saifullah, S. Gothai, M.Z. Hussein, A.K. Pandurangan, P. Arulselvan, M.E. Norhaizan, Sustained release of anticancer agent phytic acid from its chitosan-coated magnetic nanoparticles for drug-delivery system, Int. J. Nanomed. 12 (2017) 2361–2372.
[33] V. Manjusha, M.R. Rajeev, T.S. Anirudhan, Magnetic nanoparticle embedded chitosan-based polymeric network for the hydrophobic drug delivery of paclitaxel, Int. J. Biol. Macromol. 235 (2023) 123900.
[34] F. Barahuie, D. Dorniani, B. Saifullah, Palanisamy Arulselv, M.Z. Husseine, Ravindran Jaganathan, Ariyati Retno Pratiwi, Tannic acid chitosan iron oxide nanocomposite for cervical cancer treatment, Inorg. Chem. Commun. 162 (2024) 112160.
[35] S.D. Girawale, S.N. Meena, V.S. Nandre, S.B. Waghmode, K.M. Kodam, Biosynthesis of vanillic acid by Ochrobactrum anthropi and its applications, Bioorg. Med. Chem. 72 (2022) 117000.
[36] S. Taqvi, E.A. Bhat, N. Sajjad, J.S.M. Sabir, A. Qureshi, I.A. Rather, S. Rehman, Protective effect of vanillic acid in hydrogen peroxide-induced oxidative stress in D.Mel-2 cell line, Saudi J. Biol. Sci. 28 (2021) 1795–1800.
[37] M. Zhu, X. Tang, Z. Zhu, Z. Gong, W. Tang, Y. Hu, C. Cheng, H. Wang, A. Sarwar, Y. Chen, F. Liu, J. Huo, X. Wang, Y. Zhang, STING activation in macrophages by vanillic acid exhibits antineoplastic potential, Biochem. Pharmacol. 213 (2023) 115618.
[38] J. Kaur, M. Gulati, S.K. Singh, G. Kuppusamy, B. Kapoor, V. Mishra, S. Gupta, M.F. Arshad, O. Porwal, N.K. Jha, M.V.N.L. Chaitanya, D.K. Chellappan, G. Gupta, P.K. Gupta, K. Dua, R. Khursheed, A. Awasthi, L. Corrie, Discovering multifaceted role of vanillic acid beyond flavours: Nutraceutical and therapeutic potential, Trends Food Sci. Technol. 122 (2022) 187–200.
[39] S. Mohan, A. Nair, M.S. Poornima, K.G. Raghu, Vanillic acid mitigates hyperinsulinemia induced ER stress mediated altered calcium homeostasis, MAMs distortion and surplus lipogenesis in HepG2 cells, Chem. Biol. Interact. 375 (2023) 110365.
[40] V. Sathesh Kanna, S. Jagan, S. Sharmila, K. Palanisamy, S. Nirmala, T. Devaki, Vanillic acid attenuates cell proliferation, xenobiotic enzyme activity, and the status of pulmonary mitochondrialenzymes in lung carcinoma, J. Food Biochem. 46 (2022) e14366.
[41] J. Kaur, M. Gulati, K. Gowthamarajan, S. Vishwas, D.K. Chellappan, G. Gupta, K. Dua, N.K. Pandey, B. Kumar, S.K. Singh, Combination therapy of vanillic acid and oxaliplatin co-loaded in polysaccharide based functionalized polymeric micelles could offer effective treatment for colon cancer: a hypothesis, Med. Hypotheses 156 (2021) 110679.
[42] R.S. Ibrahim, A.A. El-Banna, Network pharmacology-based analysis for unraveling potential cancer-related molecular targets of Egyptian propolis phytoconstituents accompanied with molecular docking and in vitro studies, RSC Adv. 11 (2021) 11610.
[43] P. Kushwaha, P. Chauhan, Facile synthesis of water-soluble Fe_3O_4 and Fe_3O_4@PVA nanoparticles for dual-contrast T1- and T2-weighted magnetic resonance imaging, Magn. Reson. Imaging 95 (2023) 50–58.
[44] Y. Xue, B. Karmakar, J. Ke, H.A. Ibrahium, N.S. Awwad, A.F. El-kott, Immobilized Au nanoparticles on chitosan-biguanidine modified Fe3O4 nanoparticles and investigation of its anti-human lung cancer activity, J. Saudi Chem. Soc. 26 (2022) 101391.
[45] L. Martin, K. Lopez, S. Fritz, C.P. Easterling, J.A. Krawchuck, A.R. Poerwoprajitno, W. Xu, Determination of the optical interference of iron oxide nanoparticles in fluorometric cytotoxicity assays, Heliyon 10 (3) (2024) e25378.

[46] F.V. Gutierrez, I.S. Lima, A. De Falco, B.M. Ereias, O. Baffa, C.D.d.A. Lima, L.I.M. Sinimbu, P.d.l. Presa, C. Luz-Lima, Jefferson F.D.F. Araujo, The effect of temperature on the synthesis of magnetite nanoparticles by the coprecipitation method, Heliyon 10 (2024) e25781.
[47] A.R. Liandi, A.H. Cahyana, R.T. Yunarti, T.P. Wendari, Facile synthesis of magnetic FeO@Chitosan nanocomposite as environmentally green catalyst in multicomponent Knoevenagel-Michael domino reaction, Ceram. Int. 48 (2022) 20266–20274.
[48] S. Noroozi, S. Hashemnia, Z. Mokhtari, Facile synthesis of cube-shaped Fe_3O_4 mesoporous nanoparticles and their application for electrochemical determination of Cu (II) in aqueous solutions through the mediating effect of indigo carmine, Mater. Sci. Eng.: B 286 (2022) 116057.
[49] R. Wan, S. Chen, X. Tang, Z. Feng, J. Liu, Y. Li, Effect mechanism of the Fe_3O_4 nanoparticles on mechanical properties and anticorrosion performances of epoxy coatings, Prog. Org. Coat. 173 (2022) 107181.
[50] M. Khodamorady, K. Bahrami, Fe_3O_4@BNPs@ZnO–ZnS as a novel, reusable and efficient photocatalyst for dye removal from synthetic and textile wastewaters, Heliyon 9 (6) (2023) e16397.
[51] K. Saravanakumar, A. Sathiyaseelan, P. Manivasagan, M.S. Jeong, M. Choi, E.-S. Jang, V.V. Priya, M.-H. Wang, Photothermally responsive chitosan-coated iron oxide nanoparticles for enhancederadication of bacterial biofilms, Biomater. Adv. 141 (2022) 213129.
[52] N.M. El-Sayed, M.A. El Bakary, M.A. Ibrahim, M.A. Elgamal, H.E. ElZorkany, H.A. Elshoky, Synthesis and characterization of mussel-inspired nanocomposites based on dopamine–chitosan–iron oxide for wound healing: in vitro study, Int. J. Pharm. 632 (2023) 122538.
[53] M. Tabassum, M. Shahruzzaman, N.A. Mukta, S. Biswas, M.N. Khan, M.A. Kader, P. Haque, Hydroxyapatite and cellulose nanocrystals loaded gelatin-chitosan based electrospun nanofibrous mats for rapid wound healing, Heliyon 10 (4) (2024) e25871.
[54] J. Kaur, M. Gulati, P. Famta, L. Corrie, A. Awasthi, S. Saini, G.L. Khatik, V.G. Bettada, S.R.V. Madhunapantula, K.R. Paudel, G. Gupta, D.K. Chellappan, M. F. Arshad, J. Adams, K. Gowthamarajan, K. Dua, P.M. Hansbro, S.K. Singh, Polymeric micelles loaded with glyburide and vanillic acid: I. Formulation development, in-vitro characterization and bioavailability studies, Int. J. Pharm. 624 (2022) 121987.
[55] M.A. Mohammadi, S. Asghari, B. Aslibeiki, Surface modified Fe_3O_4 nanoparticles: a cross-linked polyethylene glycol coating using plasma treatment, Surface. Interfac. 25 (2021) 101271.
[56] G. Wang, F. Si, Y. Ma, Y. Wang, Z. Zhang, R. Yu, X. Zhang, G. Chang, J. Mu, H. Che, P. Li, D. Li, Fe_3O_4 nanoparticles anchoring onto graphitic carbon nitrogen nanosheets for enhanced magneto-stimuli responses and sedimentation stability, J. Mater. Res. Technol. 23 (2023) 3744–3755.
[57] M. Maruthupandy, G. Rajivgandhi, T. Muneeswaran, M. Anand, F. Quero, Highly efficient antibacterial activity of graphene/chitosan/magnetite nanocomposites against ESBL-producing Pseudomonas aeruginosa and Klebsiella pneumonia, Colloids Surf. B Biointerfaces 202 (2021) 111690.
[58] S.H. Hussein-AlAli, M.Z. Hussein, B. Saifullah, P. Arulselvan, Chlorambucil-iron oxide nanoparticles as a drug delivery system for Leukemia cancer cells, Int. J. Nanomed. 16 (2021) 6205–6216.
[59] M.K. Jabali, A.R. Allafchian, S.A.H. Jalali, H. Shakeripour, R. Mohammadinzhad, F. Rahmani, Design of a pDNA nanocarrier with ascorbic acid modified chitosan coated on superparamagnetic iron oxide nanoparticles for gene delivery, Colloids Surf. A: Physicochem. Eng. Asp. 632 (2022) 127743.
[60] S. Esthar, J. Rajesh, S. Ayyanaar, G. Gangatharan, V. Kumar, V.S. Thanigaivel, T.J. Webster, G. Rajagopal, An anti-inflammatory controlled nano drug release and pH-responsive poly lactic acid appended magnetic nanosphere for drug delivery applications, Mater. Today Commun. 34 (2023) 105365.
[61] K. Saha, K. Dutta, A. Basu, A. Adhikari, D. Chattopadhyay, P. Sarkar, Controlled delivery of tetracycline hydrochloride intercalated into smectite clay using polyurethane nanofibrous membrane for wound healing application, Nano-Struct. Nano-Objects 21 (2020) 100418.
[62] A. Sathiyaseelan, Kandasamy Saravanakumar, Arokia Vijaya, A. Mariadoss, M.-H. Wang, pH-controlled nucleolin targeted release of dual drug from chitosan-gold based aptamer functionalized nano drug delivery system for improved glioblastoma treatment, Carbohydr. Polym. 262 (2021) 117907.
[63] N.J. Prakash, D. Shanmugarajan, B. Kandasubramanian, P. Khot, K. Kodam, Biodegradable silk-curcumin composite for sustained drug release and visual wound monitoring, Mater. Today Chem. 27 (2023) 101289.
[64] V. Kumari, P. Tyagi, A. Sangal, In-Vitro kinetic release study of illicium verum (Chakraphool) polymeric nanoparticles, Mater. Today: Proc. 60 (2022) 14–20.
[65] E.R. Soltani, H. Panahi, Elham Moniri, N.T. Fard, I. Raeisi, J. Beik, A.Y. Siavoshani, Construction of a pH/Temperature dual-responsive drug delivery platform based onexfoliated MoS nanosheets for effective delivery of doxorubicin: parametric optimization via central composite design, Mater. Chem. Phys. 295 (2023) 127159.
[66] A.G. Sabzevari, H. Sabahi, M. Nikbakht, S.J.P. McInnes, Development and characteristics of layered EGCG/Montmorillonite hybrid: an oralcontrolled-release formulation of EGCG, J. Drug Deliv. Sci. Technol. 76 (2022) 103750.
[67] F. Barahuie, M.Z. Hussein, S. Abd Gani, S. Fakurazi, Z. Zainal, Synthesis of protocatechuic acid-zinc/aluminium layered double hydroxide nanocomposite as an anticancer nanodelivery system, J. Solid State Chem. 221 (2015) 21–31.
[68] F. Barahuie, M.Z. Hussein, P. Arulselvan, S. Fakurazi, Z. Zainal, Drug delivery system for an anticancer agent, chlorogenate-Zn/Al-layered double hydroxide nanohybrid synthesised using direct co-precipitation and ion exchange methods, J. Solid State Chem. 217 (2014) 31–41.
[69] H. Pelicano, D. Carney, P. Huang, ROS stress in cancer cells and therapeutic implications, Drug Resist. Updat. 7 (2004) 97–110.
[70] Y.-J. Choi, J.-H. Park, J.W. Han, E. Kim, O. Jae-Wook, S.Y. Lee, J.-H. Kim, S. Gurunathan, Differential cytotoxic potential of silver nanoparticles in human ovarian cancer cells and ovarian cancer stem cells, Int. J. Mol. Sci. 17 (2016) 2077.
[71] C.M. Neophytou, I.P. Trougakos, N. Erin, P. Papageorgis, Apoptosis deregulation and the development of cancer multi-drug resistance, Cancers 13 (2021) 4363.
[72] V. Sharma, D. Anderson, A. Dhawan, Zinc oxide nanoparticles induce oxidative DNA damage and ROS-triggered mitochondria mediated apoptosis in human liver cells (HepG2), Apoptosis 17 (2012) 852–870.
[73] G. Pistritto, D. Trisciuoglio, C. Ceci, A. Garufi, G. D'Orazi, Apoptosis as anticancer mechanism: function and dysfunction of its modulators and targeted therapeutic strategies, Aging (Albany NY) 8 (2016) 603–619.